# Adsorption of Glyphosate by Palygorskite

*Patricia Viana Rodrigues[a,b]* (ID), *Fernanda Arruda Nogueira Gomes Silva[a*]* (ID),

*Fernanda Veronesi Marinho Pontes[a]* (ID), *Carla Napoli Barbato[c]* (ID), *Viviane Gomes Teixeira[a]* (ID),

*Tainara Cristina de Assis[a,b]* (ID), *Vitor Schwenck Brandão[b]*, *Luiz Carlos Bertolino[b]* (ID)

[a]*Universidade Federal do Rio de Janeiro (UFRJ), Instituto de Química, Rio de Janeiro, RJ, Brasil.*
[b]*Ministério da Ciência, Tecnologia e Inovações (MCTI), Centro de Tecnologia Mineral (CETEM), Rio de Janeiro, RJ, Brasil.*
[c]*Instituto Federal de Educação, Ciência e Tecnologia do Rio de Janeiro (IFRJ), Campus Duque de Caxias, Duque de Caxias, RJ, Brasil.*

Glyphosate affects ecosystems due to exposure of non-target crops and is a persistent contaminant at low concentrations. The application of palygorskite to reduce glyphosate contamination in Brazil is an environmentally friendly way to remediate impacted areas. This research evaluated palygorskite application for glyphosate adsorption present in a synthetic effluent. Palygorskite samples were ore dressed by wet granulometric classification and wet magnetic separation and submitted to organophilization with cetyltrimethyl ammonium bromide solutions at concentrations of 0.01, 0.1, 1.0 and 1.5% (w/w), and the organo-palygorskite was applied in glyphosate adsorption tests. After ore dressing there was an increase in its cation exchange capacity from 19 to 41 meq 100 g$^{-1}$ and the surface area was 149 g m$^{-2}$. The 1.0% organo-palygorskite adsorbed about 86% of glyphosate from synthetic aqueous effluent. Based on this high adsorption yield, the organo-palygorskite is a potential adsorbent for remediation of effluents containing the toxic herbicide glyphosate.

**Keywords:** *Cetyltrimethyl Ammonium Bromide, Organo-Palygorskite, Toxic Herbicide Removal.*

## 1. Introduction

Glyphosate ($C_3H_8NO_5P$) or N-phosphonomethyl glycine is widely used around the world to combat weeds in agriculture. Based on its chemical structure, it is classified as an organophosphanate. It is an amphoteric compound with four acid dissociation constant values ($pk_1 = 0.8$, $pk_2 = 2.16$, $pk_3 = 5.46$ and $pk_4 = 10.14$), and is predominantly anionic in aqueous media[1].

Glyphosate is the most widely used agricultural herbicide in the world[2,3]. The indiscriminate use of this product associated with inadequate or non-existent infrastructure for washing personal protective equipment (PPE) and application machines has caused contamination of the aquatic and terrestrial environment. The International Agency for Research on Cancer of the World Health Organization has classified glyphosate as probably carcinogenic to humans, and it also has some immunotoxic effects on fish[4].

Since its commercial introduction, various methods have been applied to remove glyphosate from polluted aquatic environments, namely biological processes, physicochemical processes, advanced oxidation processes and combined water treatment processes[5].

Physicochemical processes, such as adsorption, are efficient and economical methods for pollutant removal from water and wastewater. Adsorption materials such as activated charcoal, bio-carbon, zeolite, goethite, alum sludge, graphene oxide, layered double hydroxides (LDH) and clay minerals (montmorillonite, kaolinite and illite) have been used to remove pesticides from wastewater[3,5-7].

The study of Zavareh et al.[8] of investigated the use of Cu-zeolite 4A to remove glyphosate from water at neutral pH conditions. They observed that the maximum adsorption capacity was 112.7 mg/g based on the Langmuir model. The absorption kinetics was fast, and it fitted both first- and pseudo-order models. The Cu-zeolite 4A was described as having good selectivity to glyphosate. The adsorption mechanism proposed was based on complex formation between the $Cu^{2+}$ present in the adsorbent structure and glyphosate.

The research of Mohsen Nourouzi et al.[9] applied activated charcoal derived from waste newspaper to remove glyphosate from aqueous solutions. The maximum adsorption capacity was achieved at pH 2.5 and the Langmuir adsorption isotherm was the best model to fit the experimental data.

Soares et al.[10] studied the removal of glyphosate from synthetic and wastewater samples using magnetic nanosorbents produced from magnetic cores coated with trimethyl chitosan silica hybrid shells. The removal of glyphosate from the synthetic samples was more efficient than from wastewater samples (almost 76.8% of glyphosate was removed). This result is strong evidence that the use of magnetic-assisted sorption is an efficient process to reduce the glyphosate concentration in synthetic and wastewater samples.

*e-mail: fnogueira@iq.ufrj.br

Rodrigues et al.

These studies have shown that the efficiency of the adsorption process depends on the physical and chemical structure of the solid and on the physico-chemical characteristics of the glyphosate solution. In this sense, clay minerals are excellent materials for herbicide immobilization from wastewater due to their high adsorptive and ion exchange capacities, low cost, plentiful availability and environmental stability[11].

Khenifi et al.[12] studied the removal of organophosphate and organophosphonate herbicides from aqueous solution by NiAl-LDH material. Adsorption experiments have shown two different adsorption mechanisms: external surface adsorption and interlayer anion exchange. The equilibrium adsorption data were best fitted by Langmuir isotherm. The adsorption results indicated that NiAl-LDH material is a potential adsorbent for removal of organophosphate and organophosphonate herbicides from water.

The research of Guo et al.[13] evaluated the use of kaolinite and kaolinite associated with humic acid to remove glyphosate. The kaolinite associated with humic acid adsorbed a higher concentration of glyphosate than pure kaolinite, probably due to the higher number of adsorption sites on kaolinite associated with humic acid than on pure kaolinite. Humic acid also favored the formation of H-bond networks between glyphosate and kaolinite.

Palygorskite is a clay mineral that has rarely been investigated for herbicide removal from wastewater. In some studies, it has been used as an adsorbent of organic compounds[11,14-16] and metals from wastewater[17-20]. Palygorskite has a unit cell chemical composition $[(Mg,Al)_5Si_8O_{20}(OH)_2(OH_2)_4.4H_2O]$ and fibrous morphology[17]. Its crystalline structure is formed by lamellae that are composed of one octahedral magnesium oxide layer between two tetrahedral silicon oxide layers, ordered hexagonally. This clay mineral is a type 2:1 phyllosilicate[21]. Isomorphic substitutions in its crystalline structure can occur when $Si^{4+}$ in tetrahedral sheets are changed by trivalent cations ($Al^{3+}$ or $Fe^{3+}$) and $Al^{3+}$ in octahedral sheets are changed by divalent cations ($Mg^{2+}$ and $Fe^{2+}$). This isomorphic substitution creates an excess of negative surface charge that is offset by cations ($Ca^{2+}$, $Mg^{2+}$, $Na^+$ and $K^+$) in the interlamellar space[22,23].

The physico-chemical characteristics of palygorskite, such as high specific surface area and porosity, thermal resistance, and chemical inertness, make this clay mineral potentially attractive as an adsorbent[11,20,24]. However, to use palygorskite to adsorb herbicides like glyphosate, it is necessary to modify its negative surface charge to avoid a repulsive interaction with the herbicide molecules, which normally have negative charge. Clay mineral surfaces can be modified by the introduction of long-chain organic surfactants[15,25]. The study of Dong et al.[26] proposed the thermal conditioning of a Chinese palygorskite followed by its organophilization with the cationic surfactant cetyltrimethylammonium bromide (CTAB) for the adsorption of the anionic dye Congo red. The research of Xi et al.[11] modified an Australian palygorskite with the cationic surfactants octadecyltrimethylammonium bromide and dioctadecyldimethylammonium bromide to enable adsorption of the organic herbicide (2,4-dichlorophenoxyacetic acid (2,4-D)). The organophilization of mineral materials for herbicides adsorption has been proposed in works such as that described by Chaara et al.[27] They organophilized

hydrotalcites with dodecyl sulfate ($[CH_3(CH_2)_{10}CH_2SO_4]^-$) and sebacate ($[CO_2(CH_2)_8 CO_2]^{2-}$) to evaluate which organohydrotalcites would be more efficient in adsorption of the herbicide Linuron. Results showed good efficiency for both organohydrotalcites for Linuron adsorption. However, the greatest efficiency occurred with the use of sebacate, for which the quantity of anions in the interlayer influenced the adsorptive capacity.

Brazil is a potential producer of palygorskite, although its reserves have not yet been fully estimated. The last survey in 2002, about export of the commodity, estimated reserves of 2.7 t[28]. The absence of data referring to reserves and/or production is due to the dearth of studies investigating mineral occurrences and industrial applications of this inexpensive mineral. Among the applications of palygorskite, after its chemical treatment with the use of acids, are the clarification of vegetable oils, animal tallow and carnauba wax. The export price of Brazilian palygorskite is close to US$ 130 t$^{-1}$, while the USA exports this clay mineral (as Fuller's earth) at an average price of US$ 400 t$^{-1}$ for industrial applications as adsorbents[29].

Ore dressing for the industrial application of Brazilian palygorskite as an adsorbent uses simple and low-cost techniques[22] and allows adding value to the material, improving the local economy. In addition, the possibility of regeneration and reuse of palygorskite after the adsorption process increases the interest in this material as an economically viable adsorbent[30].

The application palygorskite to reduce glyphosate contamination in Brazil is an environmentally friendly way remediate impacted areas. The consumption of glyphosate and its salts as herbicides in Brazil was estimated at 173,150.75 t in 2017 (SEI/ANVISA, 2019) and estimated worldwide at 825,804 t in 2014[31]. Since glyphosate affects ecosystems due to the exposure of non-target crops and is a persistent contaminant at low concentrations, causing severe impacts on human and animal health[28,29], the evaluation of the use of Brazilian palygorskite for the adsorption of this herbicide is attractive.

Therefore, the aim of this study was to prepare and characterize a CTAB organophilized palygorskite, obtained from the Guadalupe region of the Brazilian state of Piauí, and study its adsorption behavior versus commercial glyphosate present in a synthetic effluent.

## 2. Materials and Methods

### 2.1. Ore dressing of palygorskite

The palygorskite used in this study was collected from a mine in Guadalupe (Piauí, Brazil) and is called PALY_ROM. The PALY_ROM ore dressing was performed according to the procedure previously described by Simões et al.[22], and the fine fraction (below 20 μm) from PALY_ROM is called PALY_20.

PALY_ROM and PALY_20 samples were characterized, and organophilization and adsorption experiments were performed with PALY_20 samples.

### 2.2. Organophilization

The organophilization process was carried out with a pulp composed of PALY_20: deionized water (1:100) dispersed

by ultrasound (model C/T, Thornton–Inpec Electronica, São Paulo, Brazil) for 1 h. Subsequently, cetyltrimethyl ammonium bromide (CTAB) (Sigma-Aldrich) was added in the dispersed pulp and the pH was adjusted to 8 using ammonium hydroxide 0.77 mol $L^{-1}$ (Sigma-Aldrich) followed by homogenization by ultrasound for 3 h. Then the samples were washed with deionized water in a centrifuge (model CT-6000, CIENTEC Scientifics Equipment, Belo Horizonte, Brazil) and dried (T=50°C) in an oven (model INV-1241, Inova Sistemas Eletrônicos, Caxias do Sul, Brazil). The CTAB concentrations (% w/w) were 0.01 (PALY_201), 0.1 (PALY_202), 1.0 (PALY_203) and 1.5 (PALY_204).

After the organophilization process, PALY_201, PALY_202, PALY_203 and PALY_204 samples were characterized by X-ray diffraction (XRD), Fourier-transform infrared (FTIR) spectroscopy, surface charge (zeta potential) measurement and nuclear magnetic resonance (NMR).

## 2.3. Adsorption isotherms

In order to study the influence of initial concentration of glyphosate ($C_0$), palygorskite mass (PM), adsorption time (t), and pH on glyphosate adsorption, a $2^{1-4}$ experimental design with center point was performed.

The adsorption tests were carried out in a bath system, using PALY_203 sample and 20 mL of glyphosate solution (PESTANAL® Glyphosate, analytical standard from Sigma-Aldrich). When necessary, the pH was adjusted using sodium hydroxide or hydrochloric acid solutions (0.1 mol $L^{-1}$), The mixture was shaken for a predetermined time in a rotary shaker (T = 30°) and stirred (150 rpm). Next, the samples were centrifuged at 5,000 rpm for 4 min and filtered. Phosphorus determination in the supernatant was performed by inductively coupled plasma optical emission spectrometry (ICP OES) with a Horiba Jobin Yvon Ultima 2 spectrometer (Longjumeau, France) (Table 1 SM), where the phosphorus emission line was found to be 213.618 nm. The limit of detection and quantification (LOD and LOQ) were 0.02 mg $L^{-1}$ and 0.07 mg $L^{-1}$, respectively. The glyphosate concentration (GC) was obtained by multiplying the phosphorus concentration (PC) by the factor (F) (Equations 1A and 1B). The percentage of glyphosate adsorbed (GA) by organo-palygorskite was calculated by the difference between the initial ($GC_0$) and final concentrations ($GC_F$) of glyphosate (Equation 2).

$$GC(ppm) = PC(ppm) \times F \tag{1A}$$

$$F = \frac{glyphosate\,molar\,mass}{phosphorus\,\,molar\,mass} = \frac{169.1}{30.97} = 5.46 \tag{1B}$$

$$GA(\%) = (GC_0 - GC_F) \times 100 / GC_i \tag{2}$$

Table 1 shows the values of initial concentration of glyphosate, palygorskite mass, pH and adsorption time from the adsorption tests. Three replicates were carried out under the center point condition. The experimental data from adsorption tests were submitted to regression analysis based on an existing method for analyzing design of experiments[32]. The glyphosate adsorption (GA) data were fitted by a

**Table 1.** Variables of the $2^{1-4}$ experimental design with center point.

| Variables | Level | | |
|---|---|---|---|
| | -1 | 0 | +1 |
| Co (ppm) | 100 | 300 | 500 |
| PM (g) | 0.1 | 0.55 | 1.0 |
| pH | 3.8 | 7.4 | 11.0 |
| t (h) | 1 | 1.5 | 2 |

polynomial equation (Equation 3). The independent variables ($X_i$) were: palygorskite mass (PM), initial concentration of glyphosate ($GC_0$), pH and adsorption time (t). The estimated coefficients are represented by the indexed variable a, where $a_i$ is the linear coefficient of the variable i (palygorskite mass, initial concentration of glyphosate, pH and adsorption test duration) and $a_{ij}$ is the coefficient of the interaction between the variables i and j.

$$GA(\%) = a_0 + \sum_i^4 a_i X_i + \sum_{i<j}^4 a_{ij} X_i X_j \tag{3}$$

The optimum adsorption condition to remove glyphosate, obtained by the experimental design, was used to construct the adsorption isotherm. The isotherm data on glyphosate adsorption were fitted to the Langmuir and Freundlich equations.

The Langmuir model assumes that the surface contains a finite amount of homogeneous sites, the molecules adsorbed on them do not interact with each other, and it is only possible to form a monolayer, characterizing chemisorption. Equation 4 represents the linearized Langmuir model, where $q_e$ is the amount of solute adsorbed per gram of adsorbent at equilibrium (mg $g^{-1}$), $C_e$ is the concentration of adsorbate at equilibrium (mg $L^{-1}$), $q_m$ is maximum adsorption capacity (mg $g^{-1}$), and $K_L$ is the constant related to adsorbate binding energy in the adsorbent; or the adsorbate-adsorbent interaction constant (L $mg^{-1}$)[16,33,34].

$$C_e / q_e = (1/q_m)C_e + 1/(K_L q_m) \tag{4}$$

The characteristics of the Langmuir isotherm can be expressed by means of a dimensionless constant called the separation factor ($R_L$), which is calculated from the adsorbent/adsorbent interaction constant ($K_L$) and initial concentration ($C_0$), according to Equation 5. Adsorption is said to be favorable when the $R_L$ value is between 0 and 1. When $R_L$ is greater than 1, adsorption is said to be unfavorable and when $R_L$ is equal to 1, the isotherm is linear. The process is irreversible when $R_L$ is equal to zero[35].

$$R_L = 1/(1 + K_L C_0) \tag{5}$$

The Freundlich model can be applied to non-ideal systems, in which the adsorption sites have different energy levels, called heterogeneous sites, and it is possible to form multilayers. Due to these properties, the Freundlich model is characterized as physisorption. Equation 6 represents the linearized Freundlich model, where $q_e$ is the amount of solute adsorbed per gram of adsorbent at equilibrium (mg $g^{-1}$), $C_e$

is the concentration of adsorbate at equilibrium (mg L$^{-1}$), K$_F$ is Freundlich adsorption capacity constant (mg g$^{-1}$), and n is the Freundlich constant (dimensionless)[16,36,37].

$$logq_e = logK_F + (1/n)log C_e \qquad (6)$$

The amount of solute adsorbed per gram of adsorbent at equilibrium (q$_e$) was calculated by Equation 7, where C$_o$ is the initial concentration of adsorbate (mg L$^{-1}$), C$_e$ is the concentration of adsorbate at equilibrium (mg L$^{-1}$), V is the volume of solution (L) and m is the mass of adsorbent.

$$q_e = (C_o - C_e)V/m \qquad (7)$$

## 2.4. Characterization

The mineral constituents of the palygorskite samples were determined with a Bruker-AXS D5005 diffractometer (Germany), with CoKα radiation (35kV/40mA); 2θ path, with 1 s per path counting time and data collection from 5 to 80º (2θ). The qualitative interpretation of the spectrum was done by comparison with standards contained in the PDF02 (ICDD, 1996) using the Bruker DiffracPlus software.

X-ray fluorescence analyses were performed with an Axios$^{mAX}$ PANalytical X-ray fluorescence spectrometer (Netherlands) to ascertain the chemical composition. Samples were pressed with a Vaneox automatic press (20 mm mold, P 20 tons and t 30 s), using as binder a 1:7 mixture of boric acid (H$_3$BO$_3$) and palygorskite powder.

The thermal analysis data were collected using a Mettler Toledo TGA/DSC 1 S**TA**R$^e$ system (Mettler-Toledo AG, Analytical, Switzerland) under nitrogen atmosphere (50 mL min$^{-1}$), in the temperature range from 25 to 1000 ºC and heating rate of 10 ºC min$^{-1}$.

The cation exchange capacities of PALY_ROM and PALY_20 were determined by the methylene blue method based on the ASTM C837-09, 2009 standard.

Fourier-transform infrared (FTIR) spectra were recorded in the 4,000 to 500 cm$^{-1}$ range with a Nicolet 6700 FT-IR optical spectrometer (Thermo Fisher Scientific, USA) equipped with Fourier-transform diffuse reflectance using KBr pellets.

The textural properties of the samples were determined by nitrogen physisorption (N$_2$) at -196 ºC (77 K). The analyses were performed with an ASAP™ 2000 analyzer (Micromeritics Instrument Corporation, USA). The pretreatment of the samples consisted of drying at 200 ºC under vacuum of 1x10$^{-6}$ mmHg for 24 h to eliminate physiosorbed water. Then the adsorption and desorption isotherms were obtained by varying the partial pressure of N$_2$. With the isotherms, the surface areas were calculated using the BET method (Brunauer-Emmett-Teller) and the pore size distribution was obtained from the N$_2$ desorption isotherm by the same BET method.

The morphology of the palygorskite sample was observed by scanning electron microscopy using a Quanta™ 250 FEG microscope (Thermo Fisher, USA) operating at 20.00 kV. The samples were previously metallized with brass using a Leica EM ACE600 high vacuum sputter coater (Leica Microsystems, Wetzlar, Germany).

Surface charge (zeta potential) was determined by measuring the electrophoretic mobility with a Zetasizer Nano ZS analyzer (Malvern Panalytical, Spectris, United Kingdom and Netherlands). The suspensions were prepared with 0.05 g of sample and 10 mL of KCl (0.001 mol L$^{-1}$) and the pH values from 3 to 12 were adjusted with KOH (0.1 mol L$^{-1}$) and HCl (0.1 and 0.5 mol L$^{-1}$).

Nuclear magnetic resonance (NMR) spectra were obtained with a Bruker Avance III 9.4 Tesla wide bore solid state spectrometer (Germany) operating at 400 MHz, with maximum spinning rates of 5 kHz for NMR $^{29}$Si, 12 kHz for NMR $^{27}$Al and 10 kHz for NMR $^{13}$C.

## 3. Results and Discussion

The palygorskite obtained from Guadalupe region was first submitted to ore dressing to reduce the amount of impurities and enhance its surface properties. After physical and chemical characterization, the CTAB organophilization study was carried out. Finally, the most promising material was evaluated for the adsorption of glyphosate from synthetic effluent by the construction of Langmuir and Freundlich isotherms and analysis of their adsorption parameters.

### 3.1. Ore dressing and characterization of palygorskite

The mineral constituents of palygorskite samples were determined by X-ray diffraction. The XRD patterns of PALY_ROM and PALY_20 are shown in Figure 1 SM. For PALY_ROM and PALY_20 samples, there was a peak at 9.8° (2θ), attributed to the (110) palygorskite plane. In addition, relative peaks at 23.7° and 41° (2θ) were also observed, representing the palygorskite planes (121) and (221) respectively. These parameters were in line with the findings of Belaroui et al.[23]. The peaks at 24.27° and 31.02° (2θ) were attributed to quartz. Other impurities were observed, such as kaolinite (2θ = 14.27°) and goethite (2θ = 46.68°). After ore dressing, the patterns of the palygorskite sample (PALY_20) had smaller peaks related to quartz, kaolinite and goethite, providing evidence of reduced impurities.

Table 2 shows the elemental chemical composition, expressed in % w/w, of PALY_ROM and PALY_20, detected by X-ray fluorescence. The Al$_2$O$_3$, SiO$_2$ and MgO contents before and after ore dressing were similar. However, the SiO$_2$ content decreased to 2.8% w/w after dressing. This result indicates a reduced concentration of quartz after dressing.

The thermal analysis (from 25 to 1000 ºC) was carried out with run-of-mine and dressed ore samples, showing three mass loss events, related to dehydration, in the temperature ranges of 25 - 180, 180 – 240 and 240 - 460 ºC (Figure 2 SM). The first event is attributed to loss of water adsorbed on the surface of the clay mineral (D1)[14,22,38]; the second event is characteristic of the loss of zeolitic water present in the channels of palygorskite (D2)[22]; and the last event is related to the structural water loss from the hydroxyl groups of palygorskite (D3)[10,22,39]. According to Cheng et al.[40], the origin of the palygorskite sample and the amount of impurities are parameters that influence the result of thermal analysis. Table 3 shows that the dressed palygorskite, PALY_20, underwent greater mass loss referring to zeolitic water

**Table 2.** Chemical composition of palygorskite samples before (PALY_ROM) and after PALY_20) ore dressing.

| Samples | Teor (% w/w) | | | | | | | | | |
|---|---|---|---|---|---|---|---|---|---|---|
| | Al2O3 | SiO2 | MgO | Fe2O3 | MnO | K2O | CaO | TiO2 | L.O.I. | Total |
| **PALY_ROM** | 13.6 | 56.3 | 5.6 | 7.2 | 0.14 | 2.0 | 0.23 | 0.58 | 14.3 | 99.95 |
| **PALY_20** | 13.5 | 53.5 | 5.4 | 7.0 | 0.13 | 1.9 | 0.23 | 0.55 | 17.8 | 100.01 |

(D2) (1.57%) when compared to the PALY_ROM samples (1.29%), which is strong evidence of a higher concentration of palygorskite in the PALY_20 sample, since zeolitic water is characteristic of this clay mineral. Therefore, the ore dressing process of palygorskite was effective.

The results of the CEC analysis of the PALY_ROM and PALY_20 samples were 19 and 41 meq 100 g$^{-1}$. This indicates that the ore dressing promoted an increase in palygorskite's cation exchange capacity. According to the literature, the palygorskite CEC ranges from 30 to 50 meq 100 g$^{-1}$ [41-44]. There was a higher concentration of palygorskite in the finer fraction (PALY_20), due to removal of impurities such as quartz, goethite and kaolinite, which are minerals with very low CEC values. As mentioned, dressing can favor the adsorptive capacity of palygorskite.

The morphological study by SEM, Figure 3 SM, showed that the fibrous structure of the palygorskite was maintained after ore dressing, since the PALY_20 sample presented elongated crystals with a fibrous aspect. This is characteristic of this clay mineral, as reported in previous works[38,41,42].

The BET analysis of the PALY_20 sample revealed an average pore diameter 15 nm, which indicates predominance of mesopores[43]. The N$_2$ adsorption isotherm obtained by the BET method for the PALY_20 sample indicated Type IV isotherm and the study of its hysteresis suggested wedge-shaped pores (H3), according to the types of isotherms reported in the literature[44]. This isotherm corresponds to a mesoporous surface, corroborating the pore size value obtained[44].

The specific surface area obtained for PALY_20 was 149 m$^2$ g$^{-1}$, in accordance with the literature[45,46], while the average pore volume was 0.39 cm$^3$ g$^{-1}$. The specific surface area value for PALY_20 is considered high compared to other palygorskites also used for adsorption, such as 75, 92.94 and 135 m$^2$ g$^{-1}$ [20,38,43]. Palygorskite has higher surface area than other clay minerals such as kaolinite, illite and goethite, It can reach 210 m$^2$ g$^{-1}$, favoring application as an adsorbent[47].

The characterization of the samples suggested that the dressed palygorskite (PALY_20) was suitable for adsorption tests with the glyphosate solution due to its small particle size, high CEC and low impurity content, so it was used in the organophilization process.

## 3.2. Organophilization of dressed palygorskite

According to Simões et al.[22], a palygorskite has a negative surface charge and is hydrophilic at pH from 1 to 11. However, for application to remove organic anions such as glyphosate, it is necessary to perform organophilization, which changes its surface charge from negative to positive, with the use of a cationic surfactant, and thus promote effective interaction of the palygorskite and glyphosate molecules. Therefore, the dressed palygorskite sample and that organophilized with CTAB, as described in item 2.2, was characterized using

**Table 3.** Mass loss of samples PALY_ROM and PALY_20.

| Peak | Temperature (oC) | Mass loss (% w/w) | |
|---|---|---|---|
| | | PALY_ROM | PALY_20 |
| D1 | 25 – 180 | 8.23 | 9.43 |
| D2 | 180 – 240 | 1.29 | 1.57 |
| D3 | 240 – 460 | 1.63 | 4.58 |

XRD, FTIR, NMR, textural analysis (BET) and surface charge (zeta potential) analysis.

The XRD patterns showed no noticeable change of palygorskite before (PALY_20) and after organophilization (PALY_201, PALY_202, PALY_203 and PALY_204) (Figure 4 SM), suggesting there was no change in the crystallinity degree of the material and also no increase or decrease in the interlamellar space of palygorskite. This result corroborates those obtained by other authors[11,48]. According to Silva et al.[49], the interlamellar space of palygorskite is not modified by the addition of surfactants due to its fibrous structure, which does not allow its swelling when immersed in water.

Fourier-transform infrared spectroscopy (FTIR) was used as a complementary technique to X-ray fluorescence in the chemical characterization of the material in order to observe whether the characteristic bands of the palygorskite were maintained after organophilization and if characteristic bands of CTAB appeared. The spectra of the samples before and after organophilization (Figure 5 SM) showed the characteristic bands of the palygorskite, present at 3616 cm$^{-1}$, attributed to the Al-OH stretching (main band of palygorskite)[50], at 3413 and 3548 cm$^{-1}$, characteristic of the coordination of water molecules and zeolitic water[40,50], and at 1655 cm$^{-1}$, attributed to the deformation of water molecules[51]. Furthermore, the band at 1030 cm$^{-1}$ is characteristic of Si-O-Si vibrational stretching and that at 914 cm$^{-1}$ is attributed to Al-OH-Al deformation[40]. The band at 797 cm$^{-1}$ refers to the vibration of the Si–O bond[42], the band at 428 cm$^{-1}$ is due to the Si-O-Mg bond[52], the band at 467 cm$^{-1}$ refers to the vibration of Si-OH, and that at 513 cm$^{-1}$ is probably characteristic of Si-O-Al (IV)[49]. Finally, the bands at 424, 469, 467 and 513 cm$^{-1}$ are due to Si-O-Si vibration[53,54].

After organophilization, the FTIR spectra of PALY_201, 202, 203 and 204 samples were similar to those of the non-organophilized palygorskite (PALY_20), except for the appearance of three bands characteristic of carbon compounds. The two bands at ~ 2921 and ~ 2854 cm$^{-1}$ are characteristic of CH$_2$ asymmetric stretching vibration ($v_{as}$) and CH$_2$ symmetric stretching vibration ($v_s$), respectively. The third band, at ~ 1479 cm$^{-1}$, is attributed to CH$_2$ bending vibration and was only noted in the three samples with the highest concentrations of CTAB (PALY_202 to 204)[15,55-57].

According to the FTIR spectra, the palygorskite maintained its characteristic bonds even after organophilization,

corroborating the results of XRD analysis. These results also indicate that CTAB can interact with the aluminol (Al-OH) and silanol (Si-OH) groups of the palygorskite surface, as characterized by FTIR.

NMR was used as a complementary technique to investigate the organophilization of palygorskite. The silicon-29 ($^{29}Si$) spectra of the samples of palygorskite before and after organophilization (Figure 6 SM) showed chemical shifts at 89.3, 91.8, 93.0, 94.7, 95.9, 97.6 and 107.6 ppm, which are characteristic of Si from the tetrahedral layers of palygorskite[58]. Some noises observed in the spectra were probably due to the isomorphic substitution of $Si^{4+}$ by $Fe^{3+}$. According to the XRD results, the iron content, converted to $Fe_2O_3$, in this sample was 7.0% w/w, Table 2.

In the aluminum-27 (27Al) NMR spectra of the palygorskite samples before and after organophilization, peaks were observed regarding aluminum of the octahedral layers, with chemical shifts between 4.52 and 4.64 ppm, and of the tetrahedral layers, after isomorphic substitution of silicon atoms, with chemical shifts between 70 and 55 ppm[21,59].

The carbon-13 ($^{13}C$) spectra were obtained from pure CTAB and PALY_204 at contact times of 200 and 2,000 μs. In the pure CTAB spectrum, the signal strength was the same at both contact times, as expected, since this salt is contained in its free structure. However, in the PALY_204 spectrum, the signal was more intense for the 200 μs contact time. This result suggests there was a change in the molecular dynamics of the salt and the CTAB, probably found in the interlamellar space of the palygorskite. The signals close to 55 ppm, absent in the pure CTAB spectrum but present in the PALY_204 spectrum, indicated interaction between carbon and nitrogen atoms and the palygorskite[60].

The surface area obtained by the BET method for the samples PALY_201, PALY_202, PALY_203 and PALY_204 were 105, 68, 42, 36 m² g⁻¹, respectively. The surface area decreased as the amount of CTAB in the samples increased. The CTAB consists of a hydrophobic (nonpolar) group, with a linear hydrocarbon chain, and a hydrophilic (polar) group. The mechanism of CTAB adsorption on palygorskita is governed by the exchange of its interlayer cations by the cationic surfactant. Further interactions involving the hydrophobic chains of the adsorbed and non adsorbed CTAB species may occur and lead to the formation of multiple layers of CTAB in the solid surface. The presence of high concentration of CTAB may hind the adsorption of nitrogen molecules on palygorskita surface for BET calculations, as discussed in the FTIR, which explains the lower surface area after CTAB adsorption[61,62].

The reduction of the surface area of the organophilized palygorskite indicates a lesser adsorptive capacity of the clay mineral. However, after organophilization with the cationic surfactant, the modified material was able to adsorb to the anionic herbicide glyphosate, by means of electrostatic and intermolecular interactions and hydrogen bonds. Thus, it is necessary to evaluate the surface charge of the particles and their adsorptive capacity.

The surface charge of the dressed palygorskite and organo-palygorskites was analyzed using the zeta potential curves, Figure 1. PALY_20 had a negative charge in the studied pH
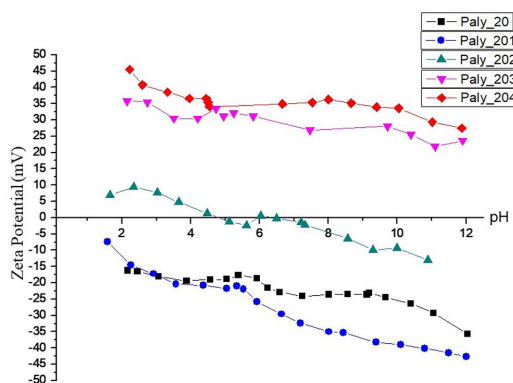


**Figure 1.** Zeta potential of dressed palygorskite (PALY_20) and organo-palygorskites (PALY_201, PALY_202, PALY_203 and PALY_204).

range (2 - 12), with values ranging from –16.2 to –35.7 mV. These results are in accordance with the literature[15,22,58,63].

A result similar to PALY_20 was obtained for the sample with 0.01% w/w of CTAB (PALY_201). This indicates that the amount of CTAB added was not sufficient to promote a change in surface charge of palygorskite. The PALY_202 sample, with 0.1% w/w of CTAB, presented positive surface charge in acidic media (pH = 1 to 6) and negative in basic media (pH = 6 to 11), presenting an isoelectric point at pH around 5. For the PALY_203 and PALY_204 (1 and 1.5% w/w of CTAB, respectively), the surface charge was positive in the pH range of 2 to 12.

By increasing the concentration of CTAB from 0.01 to 0.10% m/m for organophilization of the palygorskite, we aimed to detect a change in the surface area of the clay mineral. The result, presented in Figure 1 indicated that it increases in concentration of the surfactant promoted a change in the surface charge of the particles. Thus, we increased the surfactant concentration tem-fold (PALY_203, 1.0% m/m) with the aim of modifying the surface charge from negative to positive. Based on the favorable result, we increased the concentration only 1.5 times (PALY_204, 1.5% m/m) and observed that the zeta potential values of the sample (PALY_204) were only slightly more positive than that of the PALY_203 sample, Figure 1.

According to the results, the increase in the concentration of CTAB in the solution promoted an increase of the zeta potential. However, we suggest that at the concentration studies, the saturation of the palygorskite with the surfactant was not achieved, since the increase in the quantity adsorbed was proportional to the concentration adsorbed in the solution. Hence, we chose PALY_203 to study the adsorption of glyphosate because it was prepared with an intermediate quantity of CTAB, guaranteeing a less expensive organophilization process compared to that of PALY_204, while still containing a high level of the surfactant, which would assure that the adsorption would not be limited by this factor.

Based on these results and those reported in the literature that have confirmed the adsorptive capacity of anionic molecules in organo-palygorskite, such as 2,4-D[11], p-nitrophenol[15], red anionic dye[64], Remazol yellow GR

**Table 4.** Glyphosate adsorption values as a function of palygorskite mass, initial concentration of glyphosate, pH and adsorption test duration.

| Experiment | PM (g) | pH | t (h) | $C_0$ (ppm) | GA (%) |
|---|---|---|---|---|---|
| 1 | 0.10 | 3.8 | 1.0 | 100 | $9.4 \pm 4.5$ |
| 2 | 1.0 | 3.8 | 1.0 | 500 | $64.7 \pm 4.5$ |
| 3 | 0.10 | 11.0 | 1.0 | 500 | $29.6 \pm 4.5$ |
| 4 | 1.0 | 11.0 | 1.0 | 100 | $83.7 \pm 4.5$ |
| 5 | 0.10 | 3.8 | 2.0 | 500 | $12.5 \pm 4.5$ |
| 6 | 1.0 | 3.8 | 2.0 | 100 | $86.3 \pm 4.5$ |
| 7 | 0.10 | 11.0 | 2.0 | 100 | $27.3 \pm 4.5$ |
| 8 | 1.0 | 11.0 | 2.0 | 500 | $69.6 \pm 4.5$ |
| 9(C) | 0.55 | 7.40 | 1.5 | 300 | $61.2 \pm 4.5$ |
| 10(C) | 0.55 | 7.40 | 1.5 | 300 | $61.5 \pm 4.5$ |
| 11(C) | 0.55 | 7.40 | 1.5 | 300 | $62.3 \pm 4.5$ |

9(C), 10 (C) and 11(C): central point

dye[65] and terpenic compounds[38], we conducted tests of glyphosate in organophilized palygorskite.

## 3.3. Adsorption assays

Table 4 shows the glyphosate adsorption as a function of palygorskite mass (PM), initial concentration of glyphosate ($C_0$), pH and adsorption time (t). The empirical equation presented in this work relates the glyphosate adsorption to the experimental responses (palygorskite mass, initial concentration of glyphosate, pH and adsorption test duration). The independent variables were normalized between +1 and -1, so the parameter values could be associated with the effect variables[32].

Table 5 shows the parameters of the glyphosate adsorption equation (Equation 3) obtained from linear regression. Student's t-test was used to determine the significance of the parameter values. Whenever this significance was smaller than 5%, the parameter and regression effect were removed from Equation 3. The linear regression correlation coefficient was calculated after the removal of non-significant effects.

Equation 8 shows how the glyphosate adsorption was influenced by the experimental responses. This equation shows that palygorskite mass, pH and initial concentration of glyphosate were the variables that affected glyphosate adsorption in the range of experimental conditions analyzed, Table 2. The results of Equation 4 showed that the maximum value of glyphosate adsorption was obtained when palygorskite mass was 1.0 g; pH was 11, and initial concentration of glyphosate was 500 ppm.

$$GA = (47.4 \pm 0.2) + (56.7 \pm 0.4) \times PM + (9.7 \pm 0.4) \times$$
$$pH - (8.4 \pm 0.4) \times Co - (8.2 \pm 0.4) \times PM \times pH + \quad (8)$$
$$(1.9 \pm 0.4) \times PM \times t - (10.2 \pm 0.4) \times PM \times Co$$

The good agreement between the model and the experimental results can be observed in Figure 2, lending confidence to the empirical model (Equation 3). It is important to mention that with experimental conditions 9, 10 and 11 (center point of the experimental design), there were substantial differences between the calculated and measured glyphosate adsorption values. This is a strong indication of the existence of curvature (nonlinear behavior) in glyphosate adsorption.

**Table 5.** Estimated parameters (effect) of the experimental variables for glyphosate adsorption.

| Parameters | Values |
|---|---|
| $a_o$ | **$47.4 \pm 0.2$** |
| Curvature | **$30.5 \pm 0.8$** |
| $a_{PM}$ | **$56.7 \pm 0.4$** |
| $a_{pH}$ | **$9.7 \pm 0.4$** |
| $a_t$ | $1.7 \pm 0.4$ |
| $a_{Co}$ | **$-8.4 \pm 0.4$** |
| $a_{PM.pH}$ | **$-8.2 \pm 0.4$** |
| $a_{PM.t}$ | **$1.9 \pm 0.4$** |
| $a_{PM.Co}$ | **$-10.2 \pm 0.4$** |

PM – palygorskite mass; $C_o$ – initial concentration of glyphosate; t – adsorption test duration Significant effects are in bold (95% confidence level)
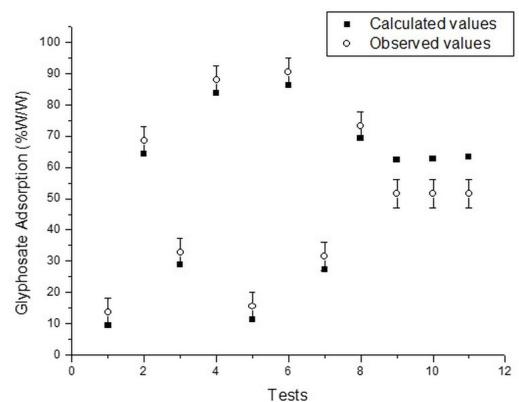


**Figure 2.** Calculated and observed glyphosate adsorption values using the empirical model (Equation 4). Error bars are confidence intervals calculated using Student's distribution with three replicas at center point and confidence level of 95%.

The analysis of the planning in the STATISTIC program indicated that the variable that most influenced the adsorption of glyphosate under the conditions in the $2^{1-4}$ experimental design was the mass of palygorskite, followed by pH and

initial concentration. The optimum adsorption condition was obtained in experiment 4 (Table 5), because it presented higher mass and pH. However, in constructing the adsorption isotherm, we used the condition of experiment 6 because it had practically the same performance as experiment 4 when the error interval was considered (4.5), as well as the greater ease of working with acidic pH, since the pH of the organophilized palygorskite in aqueous solution was approximately 3.

The adsorption isotherm was constructed by varying the initial concentration of glyphosate from 99.92 to 1,119.3 mg $L^{-1}$ under the conditions of experiment 4, i.e., 1.0 g PALY_203, 2 h stirring, pH about 3.8 and 20 mL of effluent.

Figures 3 and 4 show the Langmuir and Freundlich isotherm models, respectively. The $R^2$ values show that the two isotherm models well fitted the adsorption of glyphosate on organo-palygorskite (PALY_203), with $R^2$ values of 0.9734 and 0.9603 for the Langmuir and Freundlich models, respectively.

Based on the Langmuir model, the maximum glyphosate adsorption capacity ($q_m$) of PALY_203 was 11.69 mg $g^{-1}$.
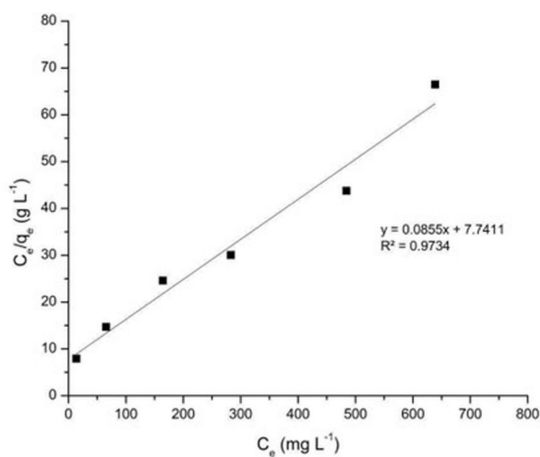


**Figure 3.** Linearized Langmuir adsorption isotherm model.
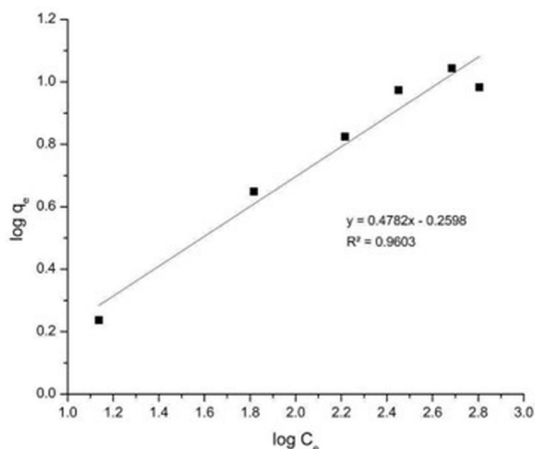


**Figure 4.** Linearized Freundlich adsorption isotherm model.

The separation factor ($R_L$) was calculated for each initial concentration of adsorption (99.92 to 1,119.3 mg $L^{-1}$) and it varied from 0.47537 to 0.07484, which suggests that the process of glyphosate adsorption in organo-palygorskite was favorable.

The Freundlich model showed an adsorption capacity constant ($K_F$) of 1.819 and a Freundlich constant (n) of 2.09 . This adsorption process is said to be favorable, since the value of n was greater than 1[66]. However, the value of $R^2$ of the Langmuir model was higher than the Freundlich model, as previously reported.

These results indicate that the adsorption of glyphosate on organo-palygorskite can occur by a chemical or physical process, since the results obtained were favorable according to both the Langmuir model and the Freundlich model. Thus, the results obtained suggest the occurrence of chemical adsorption, although an adsorption mechanism on multiple layers cannot be discarded. Furthermore, although the specific surface area of the material diminished after the organophilization, its adsorptive capacity was still high. Probably the electrostatic interactions, such as the interaction of the hydrogen bonds (as observed by Dong et al.[26]) contributed to the large improvement in the capacity for adsorption of the herbicide, with a greater influence than the decline of specific surface area.

Table 6 shows a brief overview of the adsorption parameters of some materials related in the literature and a comparison with our palygorskite organophilized in a 1.0% CTAB solution. Both Langmuir and Freundlich models are suitable for explaining the adsorption of glyphosate on a diversity of adsorbent materials. In some cases, Langmuir is slightly better than Freundlich and vice versa. Taking into account the Langmuir parameters, we can see that the values of the equilibrium constant b for the organophilized palygorskite are lower than those obtained for modified montmorillonite and graphene oxides. However, they are in the same order for those of woody biochar and $CuFe_2O_4$ and are even higher than those for zeolite 4A and graphene oxide impregnated by magnetic iron oxide nanoparticles. The adsorption capacity qm of our material was the lowest among the related materials, but we must consider that the adsorption tests were performed with the material organophilized in an only 1% CTAB solution. This choice was made based on the economical factor and constitutes the first step of our adsorption performance study, what brings the possibility of enhancing this parameter with the optimization of the whole process. The Freundlich parameters also reveal 1.0% CTAB organophilized palygorskite as a promising adsorbent material for glyphosate. The values for n indicate an efficient interaction between glyphosate and the developed adsorbent, with a significant difference being observed only when compared with montmorillonite with Fe(III).

### 3.4. Characterization of organo-palygorskite after adsorption

The palygorskite samples after adsorption of glyphosate were characterized by measurement of surface charge (zeta potential) and SEM-EDS. The zeta potential curves indicated a significant decrease in the organo-palygorskite surface charge after glyphosate adsorption in the entire pH range

(2 - 13), varying from 41.1 to 23.2 mV on PALY_203 and from 16.2 to 3.3 mV on PALY_203_GLY (after glyphosate adsorption). This is because glyphosate is predominantly negative in aqueous media, so that its interaction with the negatively charged organo-palygorskite promotes a decrease in the surface charge. In the study by Flores et al.[3], who evaluated the adsorption of glyphosate on montmorillonite, the surface charge of the clay became even more negative after the adsorption of glyphosate, since montmorillonite has a stronger negative surface charge thanpalygorskite. The research carried out by Wang et al.[72] reported that the zeta potential of goethite decreases, in modulus, with the addition of glyphosate. These results prove that organo-palygorskite was able to adsorb the glyphosate contained in synthetic aqueous effluent, since its potential also decreased, corroborating the results obtained by ICP OES.

The SEM images of the PALY_203_GLY (Figures 7 SM A and B) showed the mapping of phosphorus atoms (dots in red) on the surface of the organo-palygorskite. Phosphorus atoms refer to glyphosate since this element is present in its chemical composition. There was a homogeneous distribution of phosphorus on the surface of the organo-palygorskite, indicating the adsorption of glyphosate.

## 3.5. Advantages of the proposed adsorption process

In general, removal methods based on physicochemical processes have the advantage of low cost and adequate removal efficiency. The technology applied in this research presented a removal efficiency equal to 84-86%, with an adsorbent mass of 1 g, being considered satisfactory when compared to other examples in the literature. Table 7 shows the removal efficiency values (%) obtained from some adsorbent materials used in the literature, ranging from 73 to 100%.

For some of these materials, the narrow pH range, usually acidic, which promotes the high efficiency of the adsorbent material, becomes a disadvantage of the method[6], given the need to adjust the effluent pH in the treatment stations. As for other materials, such as graphene oxide, the recovery of the adsorbent after the removal process and the residue produced are characterized as limitations for its use[6].

The proposed adsorption process is advantageous because of its simplicity, easy operation, versatility in relation to pH (ranging from 3 to 11), for taking place at room temperature and having excellent removal efficiency. Moreover, the material presents environmental stability after disposal and the possibility of post-treatment recovery.

In addition to these advantages, the precursor material used here is low-cost and widely available in the national territory, which contributes to an interesting prognosis regarding the development of a future adsorbent material with an interesting cost. It is not yet possible to estimate the final cost of the product, as the work is still in the study phase to define the optimal amount of CTAB, the CTAB/palygorskite ratio and the technique used in the impregnation process. It is also known that the efficiency of impregnation can reduce the amount of CTAB needed and improve the performance of the material, also leading to a reduction in the costs of the organophilization step. As previously mentioned, the possibility of material regeneration and its submission to new adsorption cycles is also considered, which impacts its useful life and, consequently, the amortization of the total cost.

**Table 6.** Comparison of glyphosate adsorption parameters on some materials.

| Material | T (°C) | Freundlich constants | | | Langmuir constants | | | Ref |
|---|---|---|---|---|---|---|---|---|
| | | $K_f$ | n | $R^2$ | $q_m$ (mg g$^{-1}$) | b (L mg$^{-1}$) | $R^2$ | |
| Montmorillonite with Fe(III) | 298 | 129.693 | 9.706 | 0.922 | 202.992 | 0.983 | 0.908 | [67] |
| Graphene oxide impregnated by magnetic iron oxide nanoparticles | 298 | 24.80 | 4.55 | 0.875 | 65.402 | 0.0013 | 0.991 | [68] |
| α and δ-$Fe_2O_3$ Decorated Graphene Oxides | 298 | 11.767 | 2.92 | 0.965 | 41.925 | 0.295 | 0.988 | [69] |
| Zeolite 4A | 298 | 2.114 | 1.349 | 0.996 | 121.70 | $9.327 \times 10^{-3}$ | 0.998 | [8] |
| Woody biochar | 298 | 7.272 | 0.406 | 0.960 | 44.01 | 0.088 | 0.910 | [70] |
| $CuFe_2O_4$ | 298 | 45.929 | 3.192 | 0.979 | 302.6 | 0.023 | 0.966 | [71] |
| | 298 | 1.819 | 2.09 | 0.9603 | 11.69 | 0.0110 | 0.9734 | This work |

**Table 7.** Efficiency and pH of the adsorptive process of some materials for glyphosate removal.

| Adsorbent | pH | Removal % | References |
|---|---|---|---|
| Alum sludge | 5.2-5.6 | 99.8 | [72] |
| Graphene oxide impregnated by magnetic iron oxide nanoparticles | 4.3 | 92 | [69] |
| Graphene oxide impregnated by magnetic iron oxide nanoparticles | 3-5 | 73 | [68] |
| Activated charcoal | 8.0 | 98.45 | [73] |
| Biochar | 5.0 | 100.00 | [73] |
| Montmorillonite with Fe(III) | 1.9-4.1 | 98.05 | [67] |

# 4. Prospective Future Research

According to the results obtained for the different CTAB concentrations, a detailed kinetic study of the organophilization parameters is necessary, as well as the application of the modified material in a batch system with real effluents, and to evaluate the desorption of glyphosate to neutralize the material in subsequent adsorptive processes.

# 5. Conclusions

The ore dressing processes of the palygorskite sample from Guadalupe (Piauí, Brazil) were efficient since they provided an increase in the CEC (41 meq 100 g$^{-1}$) and the surface area (149 m2 g$^{-1}$). The dressed sample was organophilized with different concentrations of CTAB, and at 1% the change in surface charge, from negative to positive occurred in the entire pH range (2-12). This sample was used in glyphosate removal tests from aqueous media.

The maximum glyphosate removal from the effluent was about 86% and the maximum glyphosate adsorption capacity was 11.69 mg g$^{-1}$ (Langmuir model).

The analysis of the Freundlich and Langmuir isotherms showed that the glyphosate adsorption occurred by chemical, physical and physical-chemical processes. The organo-palygorskite sample after glyphosate adsorption was characterized and the results indicated a homogeneous distribution of glyphosate on the surface of the organo-palygorskite. The organophilized palygorskite proved to be a very promising material for glyphosate removal from polluted water bodies.

# 6. Acknowledgments

# 7. References

1. Li F, Wang Y, Yang Q, Evans DG, Forano C, Duan X. Study on adsorption of glyphosate (N-Phosphonomethyl Glycine) pesticide on MgAl-Layered Double hydroxides in aqueous solution. J Hazard Mater. 2005;125:89-95. http://dx.doi.org/10.1016/j.jhazmat.2005.04.037.

2. Rissouli L, Benicha M, Chafik T, Chabbi M. Decontamination of water polluted with pesticide using biopolymers: adsorption of glyphosate by chitin and chitosan. J. Mater. Environ. Sci. 2017;8:4544-9. http://dx.doi.org/10.26872/jmes.2017.8.12.479.

3. Flores FM, Torres Sánchez RM, Afonso MS. Some aspects of the adsorption of glyphosate and its degradation products on montmorillonite. Environ Sci Pollut Res Int. 2018;25:18138-46. http://dx.doi.org/10.1007/s11356-018-2073-4.

4. Arroyave JM, Waiman CC, Zanini GP, Avena MJ. Effect of humic acid on the adsorption/desorption behavior of glyphosate on goethite. Isotherms and kinetics. Chemosphere. 2016;145:34-41. http://dx.doi.org/10.1016/j.chemosphere.2015.11.082.

5. da Cruz LH, de Santana H, Zaia CTBV, Zaia DAM. Adsorption of glyphosate on clays and soils from paraná state: effect of PH and competitive adsorption of phosphate. Braz Arch Biol Technol. 2007;50:385-94. http://dx.doi.org/10.1590/S1516-89132007000300004.

6. Espinoza-Montero PJ, Vega-Verduga C, Alulema-Pullupaxi P, Fernández L, Paz JL. Technologies employed in the treatment of water contaminated with glyphosate: a review. Molecules. 2020;25:5550. http://dx.doi.org/10.3390/molecules25235550.

7. Glass RL. Adsorption of glyphosate by soils and clay minerals. J Agric Food Chem. 1987;35:497-500. http://dx.doi.org/10.1021/jf00076a013.

8. Zavareh S, Farrokhzad Z, Darvishi F. Modification of zeolite 4A for use as an adsorbent for glyphosate and as an antibacterial agent for water. Ecotoxicol Environ Saf. 2018;155:1-8. http://dx.doi.org/10.1016/j.ecoenv.2018.02.043.

9. Mohsen Nourouzi M, Chuah TG, Choong TSY. Adsorption of glyphosate onto activated carbon derived from waste newspaper. Desalination Water Treat. 2010;24:321-6. http://dx.doi.org/10.5004/dwt.2010.1461.

10. Soares SF, Amorim CO, Amaral JS, Trindade T, Daniel-da-Silva AL. On the efficient removal, regeneration and reuse of quaternary chitosan magnetite nanosorbents for glyphosate herbicide in water. J Environ Chem Eng. 2021;9:105189. http://dx.doi.org/10.1016/j.jece.2021.105189.

11. Xi Y, Mallavarapu M, Naidu R. Adsorption of the herbicide 2,4-D on organo-palygorskite. Appl Clay Sci. 2010;49:255-61. http://dx.doi.org/10.1016/j.clay.2010.05.015.

12. Khenifi A, Derriche Z, Mousty C, Prévot V, Forano C. Adsorption of glyphosate and gufosinate by Ni$_2$AlNO$_3$ layered double hydroxide. Appl Clay Sci. 2010;47:362-71. http://dx.doi.org/10.1016/j.clay.2009.11.055.

13. Guo F, Zhou M, Xu J, Fein JB, Yu Q, Wang Y, et al. Glyphosate adsorption onto kaolinite and kaolinite-humic acid composites: experimental and molecular dynamics studies. Chemosphere. 2021;263:127979. http://dx.doi.org/10.1016/j.chemosphere.2020.127979.

14. Xue A, Zhou S, Zhao Y, Lu X, Han P. Adsorption of reactive dyes from aqueous solution by silylated palygorskite. Appl Clay Sci. 2010;48:638-40. http://dx.doi.org/10.1016/j.clay.2010.03.011.

15. Sarkar B, Xi Y, Megharaj M, Naidu R, Orange II. Adsorption on palygorskites modified with alkyl trimethylammonium and dialkyl dimethylammonium bromide: an isothermal and kinetic study. Appl Clay Sci. 2011;51:370-4. http://dx.doi.org/10.1016/j.clay.2010.11.032.

16. Awad AM, Shaikh SMR, Jalab R, Gulied MH, Nasser MS, Benamor A, et al. Adsorption of organic pollutants by natural and modified clays: a comprehensive review. Separ Purif Tech. 2019;228:115719. http://dx.doi.org/10.1016/j.seppur.2019.115719.

17. Chen H, Zhao Y, Wang A. Removal of Cu(II) from aqueous solution by adsorption onto acid-activated palygorskite. J Hazard Mater. 2007;149:346-54. http://dx.doi.org/10.1016/j.jhazmat.2007.03.085.

18. Middea A, Fernandes TLAP, Neumann R, Gomes O FM, Spinelli LS. Evaluation of Fe(III) adsorption onto palygorskite surfaces. Appl Surf Sci. 2013;282:253-8. http://dx.doi.org/10.1016/j.apsusc.2013.05.113.

19. Zhu Y, Chen T, Liu H, Xu B, Xie J. Kinetics and thermodynamics of Eu(III) and U(VI) adsorption onto palygorskite. J Mol Liq. 2016;219:272-8. http://dx.doi.org/10.1016/j.molliq.2016.03.034.

20. Mohammed AA, Abdel Moamen OA, Metwally SS, El-Kamash AM, Ashour I, Al-Geundi MS. Utilization of modified attapulgite for the removal of Sr(II), Co(II), and Ni(II) Ions from multicomponent system, part i: kinetic studies. Environ Sci Pollut Res Int. 2020;27:6824-36. http://dx.doi.org/10.1007/s11356-019-07292-3.

21. Zhang Z, Wang W, Kang Y, Wang Q, Wang A. Structure evolution of brick-red palygorskite induced by hydroxylammonium chloride. Powder Technol. 2018;327:246-54. http://dx.doi.org/10.1016/j.powtec.2017.12.067.

22. Simões KMA, Novo BL, Felix AAS, Afonso JC, Bertolino LC, Silva FANG. Ore dressing and technological characterization of palygorskite from Piauí/Brazil for application as adsorbent of heavy metals. In: Ikhmayies S, Li B, Carpenter JS, Li J,

Hwang J, Monteiro SN, et al., editors. Characterization of minerals, metals, and materials 2017. Cham: Springer; 2017.

23. Belaroui LS, Ouali A, Bengueddach A, Lopez Galindo A, Peña A. Adsorption of linuron by an algerian palygorskite modified with magnetic iron. Appl Clay Sci. 2018;164:26-33. http://dx.doi.org/10.1016/j.clay.2018.03.021.

24. Ye H, Chen F, Sheng Y, Sheng G, Fu J. Adsorption of phosphate from aqueous solution onto modified palygorskites. Separ Purif Tech. 2006;50:283-90. http://dx.doi.org/10.1016/j.seppur.2005.12.004.

25. Paiva LB, Morales AR, Valenzuela Díaz FR. Organoclays: properties, preparation and applications. Appl Clay Sci. 2008;42:8-24. http://dx.doi.org/10.1016/j.clay.2008.02.006.

26. Dong W, Lu Y, Wang W, Zong L, Zhu Y, Kang Y, et al. A new route to fabricate high-efficient porous silicate adsorbents by simultaneous inorganic-organic functionalization of low-grade palygorskite clay for removal of congo red. Microporous Mesoporous Mater. 2019;277:267-76. http://dx.doi.org/10.1016/j.micromeso.2018.11.013.

27. Chaara D, Bruna F, Draoui K, Ulibarri MA, Barriga C, Pavlovic I. Study of key parameters affecting adsorption of the herbicide linuron on organohydrotalcites. Appl Clay Sci. 2012;58:34-8. http://dx.doi.org/10.1016/j.clay.2012.01.008.

28. Luz AB, Oliveira CH. Bentonita. In: Luz AB, Lins FF. Rochas & minerais industriais: usos e especificações. 2. ed. Rio de Janeiro: Centro de Tecnologia Mineral - CETEM; 2008, p. 239-54.

29. Willet JC. Clays. In: United States Department of the Interior, U.S. Geological Survey. Mineral commodity summaries. USA: U.S. Geological Survey; 2020. p. 48-50. https://doi.org/10.3133/mcs2020.

30. Li W, Liu J, Su J, Wu J, Xia Y, Zhu L, et al. An efficient and no pollutants deproteinization method for polysaccharide from arca granosa by palygorskite adsorption treatment. J Clean Prod. 2019;226:781-92. http://dx.doi.org/10.1016/j.jclepro.2019.04.092.

31. Gandhi K, Khan S, Patrikar M, Markad A, Kumar N, Choudhari A, et al. Exposure risk and environmental impacts of glyphosate: highlights on the toxicity of herbicide co-formulants. Environ. Chall. 2021;4:100149. http://dx.doi.org/10.1016/j.envc.2021.100149.

32. Box GEP, Hunter WG, Hunter JS. Statistics for experimenters: an introduction to design, data analysis, and model building. New York: Wiley; 1978.

33. Langmuir I. The dissociation of hydrogen into atoms. III. The mechanism of the reaction. J Am Chem Soc. 1916;38:1145-56. http://dx.doi.org/10.1021/ja02263a001.

34. Itodo A, Itodo H, Gafar M. Estimation of specific surface area using langmuir isotherm method. J Appl Sci Environ Manag. 2011;14. http://dx.doi.org/10.4314/jasem.v14i4.63287.

35. Erdoğan S, Önal Y, Akmil-Başar C, Bilmez-Erdemoğlu S, Sarıcı-Özdemir Ç, Köseoğlu E, et al. Optimization of nickel adsorption from aqueous solution by using activated carbon prepared from waste apricot by chemical activation. Appl Surf Sci. 2005;252:1324-31. http://dx.doi.org/10.1016/j.apsusc.2005.02.089.

36. Freundlich H. Über die adsorption in lösungen. Z Phys Chem. 1907;57U:385-470. http://dx.doi.org/10.1515/zpch-1907-5723.

37. Febrianto J, Kosasih AN, Sunarso J, Ju YH, Indraswati N, Ismadji S. Equilibrium and kinetic studies in adsorption of heavy metals using biosorbent: a summary of recent studies. J Hazard Mater. 2009;162:616-45. http://dx.doi.org/10.1016/j.jhazmat.2008.06.042.

38. Ghrab S, Eloussaief M, Lambert S, Bouaziz S, Benzina M. Adsorption of terpenic compounds onto organo-palygorskite. Environ Sci Pollut Res Int. 2018;25:18251-62. http://dx.doi.org/10.1007/s11356-017-9122-2.

39. Liu H, Chen T, Chang D, Chen D, Qing C, Xie J, et al. The difference of thermal stability between fe-substituted palygorskite

and al-rich palygorskite. J Therm Anal Calorim. 2013;111:409-15. http://dx.doi.org/10.1007/s10973-012-2363-x.

40. Cheng H, Yang J, Frost RL, Wu Z. Infrared transmission and emission spectroscopic study of selected chinese palygorskites. Spectrochim Acta A Mol Biomol Spectrosc. 2011;83:518-24. http://dx.doi.org/10.1016/j.saa.2011.08.077.

41. Murray HH. Traditional and new applications for kaolin, smectite, and palygorskite: a general overview. Appl Clay Sci. 2000;17:207-21. http://dx.doi.org/10.1016/S0169-1317(00)00016-8.

42. He D, Huang H, Xu W, Qin F, Liu S. Adsorption properties and mechanism of purified palygorskite on methylene blue. Arab J Geosci. 2018;11:658. http://dx.doi.org/10.1007/s12517-018-4015-3.

43. Thommes M, Kaneko K, Neimark AV, Olivier JP, Rodriguez-Reinoso F, Rouquerol J, et al. Physisorption of gases, with special reference to the evaluation of surface area and pore size distribution (IUPAC Technical Report). Pure Appl Chem. 2015;87:1051-69. http://dx.doi.org/10.1515/pac-2014-1117.

44. Sing KSW. Reporting physisorption data for gas/solid systems with special reference to the determination of surface area and porosity (recommendations 1984). Pure Appl Chem. 1985;57:603-19. http://dx.doi.org/10.1351/pac198557040603.

45. Galan E. Properties and applications of palygorskite-sepiolite. Clays Clay Miner. 1996;31:443-53. http://dx.doi.org/10.1180/claymin.1996.031.4.01.

46. Sylla Gueye R, Davy CA, Cazaux F, Ndiaye A, Diop MB, Skoczylas F, et al. Mineralogical and physico-chemical characterization of mbodiene palygorskite for pharmaceutical applications. J Afr Earth Sci. 2017;135:186-203. http://dx.doi.org/10.1016/j.jafrearsci.2017.08.019.

47. Shuali U, Nir S, Rytwo G. Adsorption of surfactants, dyes and cationic herbicides on sepiolite and palygorskite. In: Galàn E, Singer A. Developments in clay science. Amsterdam: Elsevier; 2011, Chapter 15, vol. 3, p. 351-74. https://doi.org/10.1016/B978-0-444-53607-5.00015-3.

48. Zhuang G, Wu H, Zhang H, Zhang Z, Zhang X, Liao L. Rheological properties of organo-palygorskite in oil-based drilling fluids aged at different temperatures. Appl Clay Sci. 2017;137:50-8. http://dx.doi.org/10.1016/j.clay.2016.12.015.

49. Silva MLG, Fortes AC, Oliveira MER, Freitas RM, Silva EC Fo, La Roca Soares MF, et al. Palygorskite organophilic for dermopharmaceutical application. J Therm Anal Calorim. 2014;115:2287-94. http://dx.doi.org/10.1007/s10973-012-2891-4.

50. Suárez M, García-Romero E. FTIR spectroscopic study of palygorskite: influence of the composition of the octahedral sheet. Appl Clay Sci. 2006;31:154-63. http://dx.doi.org/10.1016/j.clay.2005.10.005.

51. Frini-Srasra N, Srasra E. Acid treatment of south tunisian palygorskite: removal of Cd(II) from aqueous and phosphoric acid solutions. Desalination. 2010;250:26-34. http://dx.doi.org/10.1016/j.desal.2009.01.043.

52. Lazarević S, Janković-Častvan I, Djokić V, Radovanović Z, Janaćković D, Petrović R. Iron-modified sepiolite for Ni [2+] sorption from aqueous solution: an equilibrium, kinetic, and thermodynamic study. J Chem Eng Data. 2010;55:5681-9. http://dx.doi.org/10.1021/je100639k.

53. Frost RL, Locos OB, Ruan H, Kloprogge JT. Near-infrared and mid-infrared spectroscopic study of sepiolites and palygorskites. Vib Spectrosc. 2001;27:1-13. http://dx.doi.org/10.1016/S0924-2031(01)00110-2.

54. Tan L, Tang A, Zou Y, Long M, Zhang Y, Ouyang J, et al. Sb2Se3 assembling Sb2O3@ attapulgite as an emerging composites for catalytic hydrogenation of P-Nitrophenol. Sci Rep. 2017;7:3281. http://dx.doi.org/10.1038/s41598-017-03281-z.

55. Silverstein RM, Webster FX, Kiemle DJ. Spectrometric identification of organic compounds. 7th ed. Hoboken: John Wiley & Sons; 2005.

56. Huang J, Liu Y, Jin Q, Wang X, Yang J. Adsorption studies of a water soluble dye, reactive red MF-3B, using sonication-surfactant-modified attapulgite clay. J Hazard Mater. 2007;143:541-8. http://dx.doi.org/10.1016/j.jhazmat.2006.09.088.

57. Guégan R, Véron E, Forestier LL, Ogawa M, Cadars S. Structure and dynamics of nonionic surfactant aggregates in layered materials. Langmuir. 2017;33(38):9759-71.

58. Wang W, Dong W, Tian G, Sun L, Wang Q, Hui A, et al. Highly efficient self-template synthesis of porous silica nanorods from natural palygorskite. Powder Technol. 2019;354:1-10. http://dx.doi.org/10.1016/j.powtec.2019.05.075.

59. Rusmin R, Sarkar B, Biswas B, Churchman J, Liu Y, Naidu R. Structural, electrokinetic and surface properties of activated palygorskite for environmental application. Appl Clay Sci. 2016;134:95-102. http://dx.doi.org/10.1016/j.clay.2016.07.012.

60. Moura HM, Bonk FA, Pastore HO. Pillaring cetyltrimethylammonium-magadiite: a stepwise method to mesoporous materials with controlled pores sizes and distribution. Eur J Mineral. 2012;24:903-12. http://dx.doi.org/10.1127/0935-1221/2012/0024-2226.

61. Yilmaz N, Yapar S. Adsorption properties of tetradecyl- and hexadecyl trimethylammonium bentonites. Appl Clay Sci. 2004;27:223-8. http://dx.doi.org/10.1016/j.clay.2004.08.001.

62. Wang CC, Juang LC, Lee CK, Hsu TC, Lee JF, Chao HP. Effects of exchanged surfactant cations on the pore structure and adsorption characteristics of montmorillonite. J Colloid Interface Sci. 2004;280:27-35. http://dx.doi.org/10.1016/j.jcis.2004.07.009.

63. Heivilin FG, Murray HH. Hormites: palygorskite (attapulgite) and sepiolite. In: Carr DD, ed. Industrial minerals and rocks. Littleton, Colorado: Society for Mining, Metallurgy and Exploration, Inc.; 1994, p. 249-54.

64. Chen H, Zhao J. Adsorption study for removal of congo red anionic dye using organo-attapulgite. Adsorption. 2009;15:381-9. http://dx.doi.org/10.1007/s10450-009-9155-z.

65. Silva MP, Santos MFS, Santos MRMC, Santos LS Jr, Fonseca MG, Silva EC Fo. Natural palygorskite as an industrial dye remover in sigle and binary system. Mater Res. 2016;19(6):1232-40. http://dx.doi.org/10.1590/1980-5373-MR-2015-0439.

66. Vimonses V, Lei S, Jin B, Chow CWK, Saint C. Adsorption of congo red by three australian kaolins. Appl Clay Sci. 2009;43:465-72. http://dx.doi.org/10.1016/j.clay.2008.11.008.

67. Ren Z, Dong Y, Liu Y. Enhanced glyphosate removal by montmorillonite in the presence of Fe(III). Ind Eng Chem Res. 2014;53:14485-92. http://dx.doi.org/10.1021/ie502773j.

68. Li Y, Zhao C, Wen Y, Wang Y, Yang Y. Adsorption performance and mechanism of magnetic reduced graphene oxide in glyphosate contaminated water. Environ Sci Pollut Res Int. 2018;25:21036-48. http://dx.doi.org/10.1007/s11356-018-2282-x.

69. Santos TRT, Andrade MB, Silva MF, Bergamasco R, Hamoudi S. Development of α- and γ-Fe$_2$O$_3$ decorated graphene oxides for glyphosate removal from water. Environ Technol. 2019;40:1118-37. http://dx.doi.org/10.1080/09593330.2017.1411397.

70. Mayakaduwa SS, Kumarathilaka P, Herath I, Ahmad M, Al-Wabel M, Ok YS, et al. Equilibrium and kinetic mechanisms of woody biochar on aqueous glyphosate removal. Chemosphere. 2016;144:2516-21. http://dx.doi.org/10.1016/j.chemosphere.2015.07.080.

71. Jia D, Liu M, Xia J, Li C. Effective removal of aqueous glyphosate using CuFe2O4@biochar derived from phragmites. J Chem Technol Biotechnol. 2019 [cited 2022 July 26];95:196-204. Available from: https://onlinelibrary.wiley.com/doi/10.1002/jctb.6221

72. Wang Y, Ren B, Zhao Y, English A, Cannon M. A comparison of alum sludge with peat for aqueous glyphosate removal for maximizing their value for practical use. Water Sci Technol. 2018;2017:450-6. http://dx.doi.org/10.2166/wst.2018.165.

73. Dissanayake Herath GA, Poh LS, Ng WJ. Statistical optimization of glyphosate adsorption by biochar and activated carbon with response surface methodology. Chemosphere. 2019;227:533-40. http://dx.doi.org/10.1016/j.chemosphere.2019.04.078.

## Supplementary material

The following online material is available for this article:

**Table 1 SM -** Inductively coupled plasma optical emission spectrometer plasma parameters and the method used.

**Figure 1 SM -** X-ray diffraction patterns of palygorskite.

**Figure 2 SM -** Thermogravimetric curves of samples PALY_ROM and PALY_20.l

**Figure 3 SM -** SEM image of a sample of PALY_20.

**Figure 4 SM -** XRD patterns of dressed palygorskite (PALY_20) and organo-palygorskites (PALY_201, PALY_202, PALY_203 and PALY_204).

**Figure 5 SM -** FTIR spectra of the dressed palygorskite (PALY_20) and organo-palygorskites (PALY_201, PALY_202, PALY_203 and PALY_204).

**Figure 6 SM -** 29Si NMR spectra of dressed palygorskite (PALY_20) and organo-palygorskites (PALY_201, PALY_202, PALY_203 and PALY_204).

**Figure 7 SM -** A) Image obtained by SEM and B) mapping of phosphorus (red dots) of organo-palygorskite after glyphosate adsorption (PALY_203_GLY).